NI

NASA Technical Memorandum 81590

New Interpretations of Shock-Associated Noise With and Without Screech

U. von Glahn
Lewis Research Center
Cleveland, Ohio

Prepared for the
One-hundredth Meeting of the Acoustical Society of America
Los Angeles, California, November 17-21, 1980

NASA

NEW INTERPRETATIONS OF SHOCK-ASSOCIATED NOISE WITH AND WITHOUT SCREECH

by U. von Glahn

Lewis Research Center
Cleveland, Ohio

SUMMARY

Anomalous trends in present convergent nozzle (Mach 1) shock-associated noise analyses and predictions, with particular emphasis on the roles of screech and jet temperature, are discussed. Experimentally measured values of shock-associated noise are used to reassess data trends, including both frequency and sound pressure level. The data used includes model-scale nozzles, varying in nominal diameter from 5 cm to 13 cm, and full-scale engine nozzles up to 48 cm. All data were obtained at static conditions. From this reassessment of the measured data, new empirical methods for the prediction of shock-associated noise are developed. Separate procedures are presented for screech-free and screech-contaminated shock-associated noise. In the present approach, shock-associated noise spectra are developed from considerations that include the peak sound pressure level and its frequency, the low frequency sound pressure level slope, and the high frequency sound pressure level slope or roll-off; the latter is shown to vary with directivity angle.

INTRODUCTION

In many gas turbine engines, the core flow exhausts at above-critical pressures, hence at supersonic velocities. With a convergent exhaust nozzle, also referred to as a Mach 1 nozzle in the literature, the jet is imperfectly expanded. The rapid variation in pressure across the nozzle exit plane, according to reference 1, is accomplished by means of steady compression or expansion waves that propagate downstream producing the characteristic system of shock cells. These shock cells are responsible for two noise sources, (1) screech tones and (2) shock-associated noise.

Screech consists of a discrete spectrum of harmonically related tones and is an acoustic feedback phenomenon between the shock cells and the nozzle exit. It is also stated in reference 1 that screech in hot jets is not usually significant.

When the system of shock cells is sufficiently extensive (pressure ratio significantly above choke), shock-associated noise characterized by a broadband, strongly peaked spectrum is produced. This type of noise has been studied experimentally in reference 2. From these data, an empirical model of shock-associated noise has been developed in the reference. This work does not appear to depend on the stagnation temperature of the jet or the jet mixing velocity. The empirical model proposed was developed by extending a model for screech proposed in reference 3.

In recent years, a significant increase in the shock-associated noise data bank has been obtained, particularly at elevated jet temperatures, whereas many of the previous studies were made with cold flow. It has also been demonstrated (refs. 4 to 7) that the feedback loop associated with screech is easily broken by disrupting the smooth trailing edge of the nozzle by the use of tabs at the nozzle exit. Care, however, must be exercised to insure that these tabs do not adversely affect the jet mixing noise and the aerodynamics of the flow, and that their presence does not cause additional shock-associated noise (ref. 7).

On the basis of the latest studies (refs. 4 to 9), some of the original concepts and proposed trends with flow conditions, as discussed later, no longer appear to be valid. In the present study, experimentally measured values of shock-associated noise are used to reassess data trends, including both frequency and sound pressure level. The data bank used includes model-scale nozzles, varying in nominal diameter from 5 cm to 13 cm, and full-scale engine data obtained with nozzles up to 48 cm in diameter. All these data were measured at static conditions. From this reassessment and interpretation of the measured data, new empirical methods for the prediction of shock-associated noise are developed. Separate procedures are presented for screech-free and screech-contaminated shock-associated noise. In the present approach, shock-associated noise spectra developed from considerations that include the peak sound pressure level and its frequency, the low frequency sound pressure level slope, and the high frequency sound pressure level slope or roll-off.

BACKGROUND

With cold flow, screech tones are easily identified in jet noise spectra. A typical example of a broadband screech tone is shown in figure 1 in which the sound pressure level is shown as a function of frequency at a 40^{o} directivity angle. The data shown are for a 9.5 cm diameter nozzle operated with a nominal pressure ratio of 2.75 (ref. 10). Screech tones are generally omni-directional so that screech-tone data obtained at one directivity angle are similar to those at different angles. In reference 8, narrowband analysis (20 Hz) at $\theta = 45^{o}$ were performed to identify the screech tones for a convergent (Mach 1.0) nozzle. The results of the measured screech frequencies were presented in terms of Helmholtz number $H = f_s D/a_o$. The plot, reproduced from reference 8, is given in figure 2. Superimposed on the narrowband data are the identifiable screech tones observed in the broadband data of reference 10, and unpublished NASA data obtained with 7.6- and 10.2-cm diameter convergent nozzles. The broadband screech data fall well within the range of the narrowband measurements.

As has been discussed in the literature (refs. 4-7), screech tones can be suppressed by interrupting the feedback mechanism between the shock cells and the nozzle exit through the use of one or more tabs at the nozzle lip. In both references 4 and 7 a single rectangular tab was used to suppress screech The rectangular tab had dimensions of 0.125 D wide by 0.063 D long. Comparisons of screech-free and screech-contaminate shock-associated noise are illustrated in figure 3, taken from reference 7. In general, the tab eliminated the screech tone; however, the broadband jet noise can be somewhat by such a device (ref. 7).

A frequency parameter for the peak sound pressure level, SPL_p, for shock-associated noise is commonly given in the literature by:

$$f_p \sim \frac{U_c}{\beta D}\left[F\left(\frac{U_c}{a_o},\ \cos\theta\right)\right]^{-1} \tag{1}$$

where U_c is equal to a constant $\times$ U_j. The frequency, f_p, is defined as that frequency associated with the peak SPL in the shock-associated spectrum (SPL_p). Hereinafter, f_p is called peak frequency. Equation (1) suggests that the peak frequency, f_p, increases with increasing convective velocity (or jet velocity) and decreases with increasing values of jet Mach number (indicated by β) and nozzle size, D. The peak frequency also varies inversely with the directivity angle, θ.

A representative equation of the peak frequency for shock associated noise in the literature includes the following:

$$f_p = C\left(\frac{U_j}{\beta D}\right)\left[\left(1 + 0.7\left(\frac{U_j}{a_o}\right)\cos\theta\right)^{-1}\right] \tag{2}$$

The coefficient C varies with the investigator, ranging from 0.763 in reference 2 to 0.91 in reference 11.

Examination of equation (2) indicates that f_p becomes negative when the product of $0.7(U_j/a_o)\cos\theta$ exceeds -1.0, as it can in the rear quadrant ($\theta > 90^o$). The variation of f_p with θ are given in figure 4 for jet velocities of 444 and 922 m/sec, a β of 0.83, a nozzle diameter of 9.5 cm and C = 0.91. At the lower jet velocity of 444 m/sec (fig. 4(a)), the peak frequency is positive at all angles because $0.7(U_j/a_o)\cos\theta$ does not exceed -1.0; the limiting value for the example is -0.91. However, at the higher jet velocity of 922 m/sec, this term exceeds -1.0 at a θ of about 122^o (fig. 4(b)); hence, peak frequencies would be negative at angles greater than 122^o. This appears unreasonable from physical considerations.

In order to overcome this deficiency in the formulation of the equation for the peak frequency, an additional term was included in reference 12 where f_p is given by:

$$f_p = C\left(\frac{U_j}{\beta D}\right)\left[\sqrt{\left(1 + 0.7\,\frac{U_j}{a_o}\cos\theta\right)^2 + 0.04\,(U_j/a_o)^2}\right]^{-1} \tag{3}$$

with C = 0.7 instead of 0.91 as in equation (2). The variation of f_p with θ is also shown in figure 4 for the same conditions as those used with equation (2). In general, equations (2) and (3) yield the same trends of f_p with θ in the front quadrant ($\theta < 90^o$), however, the computed f_p values will be somewhat higher using equation (3) than those obtained with equation (2). Basically these trends show an increase in f_p with increasing θ. In the rear quadrant, the peak frequencies computed with equation (2) will be considerably lower than those obtained using equation (3). With equation (3) a reversal in the curve occurs as θ approaches 180^o. This reversal as a function of U_j/a_o. A typical inflection point and curve reversal is shown in figure 4(b). Such a characteristic of the peak frequency variation with

directivity angle does not appear to be supported by the available experimental evidence.

In the preceding formulations for f_p, no distinction was made between screech-free and screech-contaminated shock associated noise. As will be shown later, differences do exist.

PEAK SHOCK-ASSOCIATED SOUND PRESSURE LEVEL FREQUENCY

As has been shown in the literature (e.g., ref. 7) the presence of a screech mode in the spectrum is easily observed with cold flow and low β-values but is also present, as will be shown, with heated flow and/or at high β-values. As discussed earlier, a tab at the nozzle lip will eliminate the screech and its affect on shock-associated spectra. In the following sections, the relationships of the f_p with θ will be developed for both screech-free and screech-contaminated shock associated noise. The f_p values indicated will be for the shock spectra, not the screech tone.

Screech-free f_p. - Values of f_p taken from the screech-free model data of reference 4 are shown in figure 5 as a function of $U_j/\beta D$ for several directivity angles, θ. The data shown include variations in U_j/a_o ranging from 0.9 to 1.8. It is seen that f_p decreases with decreasing angles for constant values of $U_j/\beta D$. The line drawn through the data at $\theta = 90^o$ established a slope with $C = 0.8$. The slopes of the remaining lines shown vary from the $\theta = 90^o$ line by $(1 + \cos \theta)$. Good agreement is apparent between the measured data and the lines generated by using the following equation for determining the f_p for screech-free, broadband shock-associated noise:

$$f_p = 0.8(U_j/\beta D)(1 + \cos \theta)^{-1} \qquad (4)$$

A comparison of the f_p versus θ curve resulting from the use of equation (4) with those previously shown in figure 4(b) is shown in figure 6. The same curve using equation (4) would occur at all $U_j/\beta D$ values. Thus, the shape variations produced by the use of equations (2) and (3) have been eliminated.

Screech-contaminated f_p. - Values of f_p as a function of $U_j/\beta D$ at $\theta = 90^o$ are shown in figure 7(a). The data shown are taken from several references, as indicated in the figure. The solid line is that for screech-free f_p values taken from figure 5. It is apparent that, for equal values of $U_j/\beta D$, the screech-contaminated f_p are significantly less than those without screech. A curve faired through the screech-contaminated data suggests a constant of $C = 0.6$ compared to the value of $C = 0.8$ for the screech-free data (eq. (4)). At directivity angles other than 90^o, the trends between the screech-free and screech-contaminated f_p values are similar. For example, a comparison of f_p values at $\theta = 60^o$ is shown in figure 7(b). The dashed line through the data is obtained using the constant of $C = 0.6$ determined from the data at $\theta = 90^o$ and using the relationship $(1 + \cos \theta)^{-1}$ as in equation (4). The data in figures 7(a) and (b) are for model-scale nozzles. In figure 7(c), similar data are shown for full-scale engine nozzles (ref. 12) at a nominal θ of 50^o. On the basis of the data shown in figure 7, the f_p

for screech-contaminated, shock-associated noise can be estimated with the following equation:

$$f_p = 0.6(U_j/\beta D)(1 + \cos\theta)^{-1} \qquad (5)$$

PEAK SHOCK-ASSOCIATED SOUND PRESSURE LEVEL

Screech-Free SPL_p

In the development of the present analysis, it is assumed that the variations of both the peak sound pressure levels, SPL_p, and the overall sound pressure levels, OASPL, with the jet Mach number parameter, β, are similar. The variation of OASPL with β given in reference 9 for the case of cold flow and a directivity angle, θ, of 45^o is shown in figure 8. From these measured data, an empirical relationship was obtained yielding the curve shown in the figure. This empirical relationship is expressed by:

$$OASPL_{\theta=45^o} = 118.5 + 20 \log \beta - 10 \log \left[1 + \frac{0.105}{(\beta)^{3.67}}\right] \qquad (6)$$

Also indicated in the figure by the two dash lines are the slopes (not absolute values) of simple approximations for the variation of OASPL (hence SPL_p) with β. In the region $0.4 < \beta < 0.9$ the variation of OASPL with β is approximated by β^4. In the region of $\beta > 0.9$, the approximation is given by β^2. These exponents of β have been used by some investigators to describe the variation of SPL_p with β. It is further assumed that with heated jet flows, the trend of the OASPL with β is also given by equation (6), although the constant, 118.5, in equation (6) will change with jet temperature.

In terms of SPL_p, an effective sound pressure level parameter is used herein designated SPL_p^*. This latter term is defined as:

$$SPL_p^* = SPL_p - 20 \log D/R - F_1(\beta) \qquad (7)$$

where $F_1(\beta)$ is given by:

$$F_1(\beta) = 20 \log \beta - 10 \log \left[1 + \frac{0.105}{(\beta)^{3.67}}\right] \qquad (8)$$

The variation of SPL_p with θ is shown in figure 9, the data being taken from reference 4. The curves shown in figure 9 are based on a simple 10 log (1 + cos θ) relationship and fit the data well. This directivity term is now incorporated into equation (7) yielding:

$$SPL_p^* = SPL_p - 20 \log D/R - 20 \log \beta + 10 \log \left[1 + \frac{0.105}{(\beta)^{3.67}}\right] - 10 \log(1 + \cos\theta) \qquad (9)$$

Thus far, the analysis has dealt with cold jet flows. When the measured SPL_p values of shock-associated noise are plotted in terms of equation (9) as a function of jet static-to-ambient temperature ratio, T_j/T_o, the SPL_p^* values first increase with increasing temperature ratio and then decrease (fig. 10). Also the data show a dependency on the jet Mach number parameter, β. The data can be fitted empirically by the curve shown in figure 11 using the following relationship:

$$SPL_p^* = 153.3 - 15 \log F_2(\beta) - 10 \log \left[1 + \frac{0.7}{(F_2(\beta))^{4.5}}\right] \tag{10}$$

where

$$F_2(\beta) = (T_j/T_o)/\beta(1 + 0.375\beta^3) \tag{11}$$

By combining equations (9) to (11), the value of SPL_p can be calculated by:

$$SPL_p = 153.3 - 15 \log \left[\frac{T_j/T_o}{\beta(1 + 0.375\beta^3)}\right] - 10 \log \left[1 + 0.7 \left(\frac{\beta(1 + 0.375\beta^3)}{T_j/T_o}\right)^{4.5}\right]$$

$$+ 20 \log D/R + 20 \log \beta - 10 \log \left[1 + \frac{0.105}{(\beta)^{3.67}}\right] + 10 \log(1 + \cos \theta) \tag{12}$$

Screech-Contaminated SPL_p

The analysis procedure for screech-contaminated shock-associated SPL_p is identical to that used for screech-free shock noise in the preceding section. In figure 12 is shown the variation of SPL_p^* with the previously introduced parameter $T_j/T_o/\beta(1 + 0.375\beta^3)$. The data shown include both model-scale results and those from two engine tests (Orenda engine used in the F-86 aircraft (ref. 12) and the J-85 engine used on the Aerotrain (ref. 12). The data show the same trend with temperature ratio as that with the screech-free data in the preceding section. The solid curve shown in the figure is given by:

$$SPL_p^* = 154.3 - 15 \log F_2(\beta) - 10 \log \left[1 + \frac{2.7}{(F_2(\beta))^{4.5}}\right] \tag{13}$$

where $F_2(\beta)$ is given by equation (11). This equation is similar to equation (10) except for the constants. Also shown for comparison in figure 12 by the dotted line is the curve for screech-free shock-associated SPL_p^*. A comparison of the two curves shown indicates that the screech-contaminated

shock noise is less than that for screech-free shock noise at temperature parameter values less than about 1.55. At temperature parameter values greater than 1.55 the opposite trend occurs.

On the basis of the relationships shown in figure 12, the following equation can be used to estimate screech-contaminated shock-associated peak sound pressure levels:

$$SPL_p = 154.3 - 15 \log \left[\frac{T_j/T_o}{\beta(1 + 0.375\beta^3)} \right] - 10 \log \left[1 + 2.7 \left(\frac{\beta(1 + 0.375\beta^3)}{T_j/T_o} \right)^{4.5} \right]$$

$$+ 20 \log D/R + 20 \log \beta - 10 \log \left[1 + \frac{0.105}{(\beta)^{3.67}} \right] + 10 \log(1 + \cos \theta) \qquad (14)$$

SHOCK-ASSOCIATED NOISE SPECTRAL SHAPE CHARACTERISTICS

On the basis of the data referenced herein, the spectral shape characteristics are substantially the same for both screech-free and screech-contaminated spectra. Consequently, the same empirical relationships are assumed herein to apply to both spectra.

A representative screech-free shock-associated noise spectrum (ref. 4) is shown in figure 13. The spectrum shown has the jet mixing noise subtracted from the total measured SPL values. The following sections describe the spectral characteristics in two regions: (1) that portion of the spectrum in which $f < f_p$, and (2) that portion of the spectrum in which $f > f_p$.

Lower frequency forward spectrum, $f < f_p$. - In general, the data indicate that the shock-associated SPL in the lower frequency forward portion of the spectrum increases with frequency at a rate of about 21 dB/octave band. This rate appears to be independent of all the variables included in the data bank.

Higher frequency aft spectrum, $f > f_p$. - In the higher frequency aft portion of the spectrum, the shock-associated SPL decreases with increasing values of frequency. The variation of SPL with frequency, however, appears to be a function of the directivity angle. A typical variation of the change in the SPL/f slope with θ is shown in figure 14. It is apparent that the slope of SPL/f has decreased with a change in θ from 45^o to 90^o. Although the data shown in figure 14 are for screech-free shock-associated noise, similar results were obtained with screech-contaminated shock noise. This is to be expected because introduction of the tab that eliminated screech in these data did not affect the higher frequency portion of shock-associated noise spectrum (ref. 7).

Examination of the higher frequency aft portion of the shock-associated spectral data indicated a temperature dependency of the aft SPL slope. Typical aft SPL data (ref. 10) in terms of dB/octave band slope as a function of temperature ratio, T_j/T_o for three representative directivity angle ($\theta = 20^o$, 60^o, and 90^o) are shown in figure 15. It is apparent from these data that the

aft spectral slope becomes steeper, i.e., greater negative values of dB/octave band with increasing temperature ratio. The dB/octave band varies with $(T_j/T_o)^{0.25}$ as shown by the solid curves in the figure. The aft spectral slope data from reference 10 are replotted in figure 16 in terms of (dB/octave band)/$(T_j/T_o)^{0.25}$ as a function of T_j/T_o. On the basis of this data plot, an equation was developed to correlate this term with directivity angle. The correlation equation is given by:

$$\frac{\text{(dB/octave band)}}{(T_j/T_o)^{0.25}} = -2.75\left(\cos\frac{\theta}{2}\right) - 0.095(1 + \cos)^5 \qquad (15)$$

The solid curves in figure 16 were obtained using equation (15). In general, the comparison between the calculated curves and the data are good. This is further shown in figure 17 where the data are plotted in terms of (dB/octave band)/$(T_j/T_o)^{0.25}$ as a function of directivity angle, θ. Shown for the data at each angle is a mean value and the range of the data shown in figure 16. Also shown is the curve calculated using equation (15). Although the data deviate somewhat from the calculated curve at $\theta = 40^o$ and 60^o, this may be the result of attempting to establish a precise data slope from the experimental data.

COMPARISONS OF MEASURED AND CALCULATED SPECTRA

In the following sections, representative measured spectra at selected directivity angles from 40^o to 90^o will be compared with those synthesized by the techniques discussed herein. The synthesized spectra are developed from the following procedure:

(1) The SPL_p and f_p are calculated from equations (12) and (4), respectively for screech-free shock associated noise or from equations (14) and (5), respectively for screech contaminated shock-associated noise. These calculations yield the apex of the spectral shape.

(2) The low frequency portion of the spectral shape is obtained using a constant 21 dB/octave band slope through the previously calculated spectral apex (SPL_p and f_p).

(3) The aft spectral roll-off is calculated using equation (15). The roll-off is initiated at the spectral apex (SPL_p and f_p).

Based on this procedure, both screech-free and screech-contaminated, synthesized shock-associated spectra are compared with data from references 4 and 10 in figures 18 to 20. The data shown have the jet mixing noise subtracted from the total measured SPL values.

Screech-free spectra. - In figure 18 is shown a comparison of the measured and calculated spectra for selected flow conditions. The data are taken from reference 4. The spectra shown are for a $\beta = 0.94$ and jet velocities of 341, 538, and 601 m/s. The corresponding T_j/T_o ratios are 0.73, 1.82, and 2.27, respectively. The calculated spectra are for θ of 45^o, 60^o, and 90^o, with data shown where available. It is apparent that, in general, good agreement exists between the measured and calculated spectra.

In figure 19, a spectral comparison is shown for a $\beta = 1.34$, a jet velocity of 587 m/s and a T_j/T_o ratio of 1.82. Good agreement between the measured (ref. 4) and calculated spectra is again evident.

Screech-contaminated spectra. - In figure 20 is shown a comparison of the measured and calculated screech-contaminated spectra for selected flow conditions. The spectra shown are for $\beta = 0.83$ and jet velocities of 337, 540, and 746 m/s. The T_j/T_o ratios are 0.72, 1.52, and 2.96, respectively. The data shown are from reference 10. The agreement between the measured and calculated values is again as good as that for the screech-free data.

CONCLUDING REMARKS

On the basis of the present analysis of available shock-associated noise, it appears that, unless screech tabs were used, the measured data were contaminated by screech. The data also indicate that nozzle size (scale) is not a factor as to whether or not screech contaminates the shock-associated noise since the noise measurements included nozzles ranging from 5 to 48 cm in diameter. The data analysis also appears to indicate that screech persists even at elevated jet static temperatures and high pressure ratios. At these latter conditions screech is almost unnoticeable. In all cases where screech appears to influence the shock-associated noise, the spectra peak at a lower frequency, by 1/3- to 2/3-octave band, than those that are screech-free. Finally, it is apparent from this study that the rigs used in the several experimental programs were not a factor in the shock-associated data.

It should be pointed out that, to the best of the author's knowledge, all the nozzles included herein have smooth contours at the exit plane. It is not known, at this point, if a full-scale variable area nozzle consisting of overlapping metal leaves or "feathers" would constitute the equivalent of tabs on a screech-free nozzle. The irregularities caused by the leaves or "feathers" on the nozzle exit could help to eliminate the feedback loop between the shock cells and the nozzle lip. The experiments performed with various screech-elimination devices in reference 6 would tend to support the assumption that such nozzles are screech-free.

SUMMARY OF RESULTS

Empirical correlations have been developed that can be used to synthesize and predict both screech-free and screech-contaminated shock-associated spectra. The predicted spectra are in good agreement with the measured data and reflect trends implicit in the data, including the following:

1. The peak shock-associated sound pressure level SPL_p, varies with jet Mach number parameter β, where β is defined by $\sqrt{M_j^2 - 1}$. For jet Mach numbers, M_j, less than about 1.4, the SPL_p variation is approximated by β^4 whereas for M_j values greater than about 1.4, the variation is approximated by β^2. An equation was developed herein to provide for the continuous variation of SPL_p with β.

2. The peak sound pressure level, SPL_p, varies with jet static temperature. At low jet static temperatures, the SPL_p increases with the temperature; however, at high jet static temperatures the SPL_p decreases with temperature. An equation was developed to reflect this trend.

3. The frequency associated with SPL_p is greater by a factor of 1.33 for screech-free cases than those for screech-contaminated cases.

4. The spectral characteristics at frequencies less than that at the SPL_p value vary with an apparent dB/octave band slope of 21. At frequencies greater than the frequency at SPL_p, the spectral characteristics are a function of jet static temperature and directivity angle, θ. An equation was developed to reflect this trend in the data.

5. The variation of both the SPL_p and its associated frequency with directivity angle, θ, is given by $(1 + \cos \theta)$.

SYMBOL LIST

(All symbols are in SI units except as noted.)

a_o	ambient speed of sound
C	constant
D	nozzle diameter
F, F_1, F_2	function
f	1/3-octave band frequency
f_p	peak sound pressure level frequency
f_s	screech frequency
H	Helmholtz number, $f_s D/a_o$
M_j	jet Mach number
OASPL	overall sound pressure level, dB re $20\mu N/m^2$
R	distance from nozzle exit to microphone locations
SPL	sound pressure level, dB re $20\mu N/m^2$
SPL_p	peak sound pressure level, dB re $20\mu N/m^2$
SPL_p^*	sound pressure level parameter
T_j	jet static temperature
T_o	ambient temperature

U_c	convective velocity, constant $\times U_j$
U_j	jet velocity
β	Mach number parameter, $\sqrt{M_j^2 - 1}$
θ	directivity angle measured from inlet

REFERENCES

1. M. S. Howe and J. E. Ffowcs Williams, "On the Noise Generated by an Imperfectly Expanded Supersonic Jet," Philos. Trans. Roy. Soc. London, Series A, 289, 271-314 (1978).

2. M. Harper-Bourne and M. J. Fisher, "The Noise from Shock Waves in Supersonic Jets," in Noise Mechanisms, AGARD-CP-131 (1974), Paper 11, pp. 1-13.

3. A. Powell, "On the Mechanism of Choked Jet Noise," Proc. Phys. Soc., B, 66, 1039-1056 (1953).

4. B. J. Tester, P. J. Morris, J. C. Lau, and H. K. Tanna, "The Generation, Radiation and Prediction of Supersonic Jet Noise," AFAPL-TR-78-85-Vol. 1 (1978).

5. H. K. Tanna, "An Experimental Study of Jet Noise, Part II: Shock Associated Noise," J. Sound Vib., 50, 3, 429-444 (1977).

6. H. Kozlowski and A. B. Packman, "Flight Effects on the Aerodynamic and Acoustic Characteristics of Inverted Profile Coannular Nozzles," NASA CR-3018 (1978).

7. T. D. Norum and J. M. Seiner, "Location and Propagation of Shock Associated Noise from Supersonic Jets," AIAA Paper No. 80-0983 (June 1980).

8. J. M. Seiner and T. D. Norum, "Experiments of Shock Associated Noise on Supersonic Jets," AIAA Paper No. 79-1526 (July 1979).

9. J. M. Seiner and T. D. Norum, "Aerodynamic Aspects of Shock Containing Jet Plumes," AIAA Paper No. 80-0965 (June 1980).

10. U. von Glahn, D. Groesbeck, and J. Wagner, "Wing Shielding of High-Velocity Jet and Shock-Associated Noise With Cold and Hot Flow Jets," NASA TM X-73428 (1976).

11. P. R. Knott, J. T. Blozy, and P. S. Staid, "Acoustic and Aerodyanic Performance Investigation of Inverted Velocity Profile Coannular Plug Nozzles; Comprehensive Data Report, Vol. 1," R79AEG166-Vol-1, General Electric Co., Cincinnati, OH, (1979). NASA CR-159575-Vol-1, (1979).

12. J. R. Stone and F. J. Montegani, "An Improved Prediction Method for the Noise Generated in Flight by Circular Jets," NASA TM-81470 (1980).

13. H. Kozlowski and A. B. Packman, "Aero-Acoustic Tests of Duct-Burning Turbofan Exhaust Nozzles; Comprehensive Data Report, Vol. 1," PWA-5336-VOL-1, Pratt and Whitney Aircraft Group, East Hartford, CT, (1977). NASA CR-134910-Vol-1, (1977).

14. R. S. Larson, D. P. Nelson, and B. S. Stevens, "Aerodynamic and Acoustic Investigation of Inverted Velocity Profile Coannular Exhaust Models and Development of Aerodynamic and Acoustic Prediction Procedures; Comprehensive Data Report, Vol. II," PWA-5550-17-Vol-2, Pratt and Whitney Aircraft Groups, East Hartford, CT, (1979). NASA CR-159516, (1979).

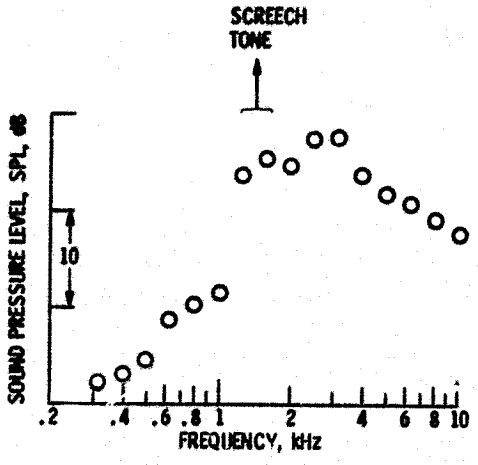

Figure 1. - Representative broadband spectrum showing presence of screech tone. Ref. 10; cold flow; $\beta = 0.83$; $\theta = 40^0$.

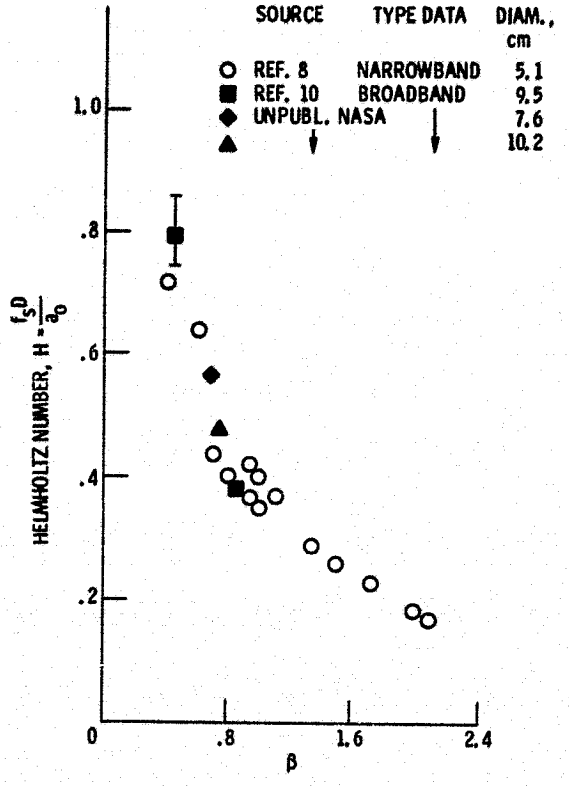

Figure 2. - Screech tones for convergent (Mach 1) nozzle.

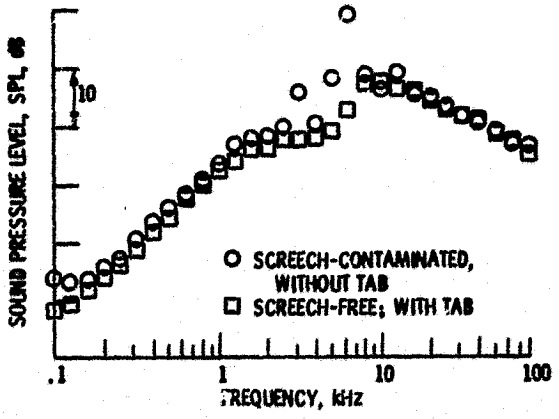

Figure 3. - Comparison of spectra with and without screech tab. $\beta = 0.94$; ref. 7.

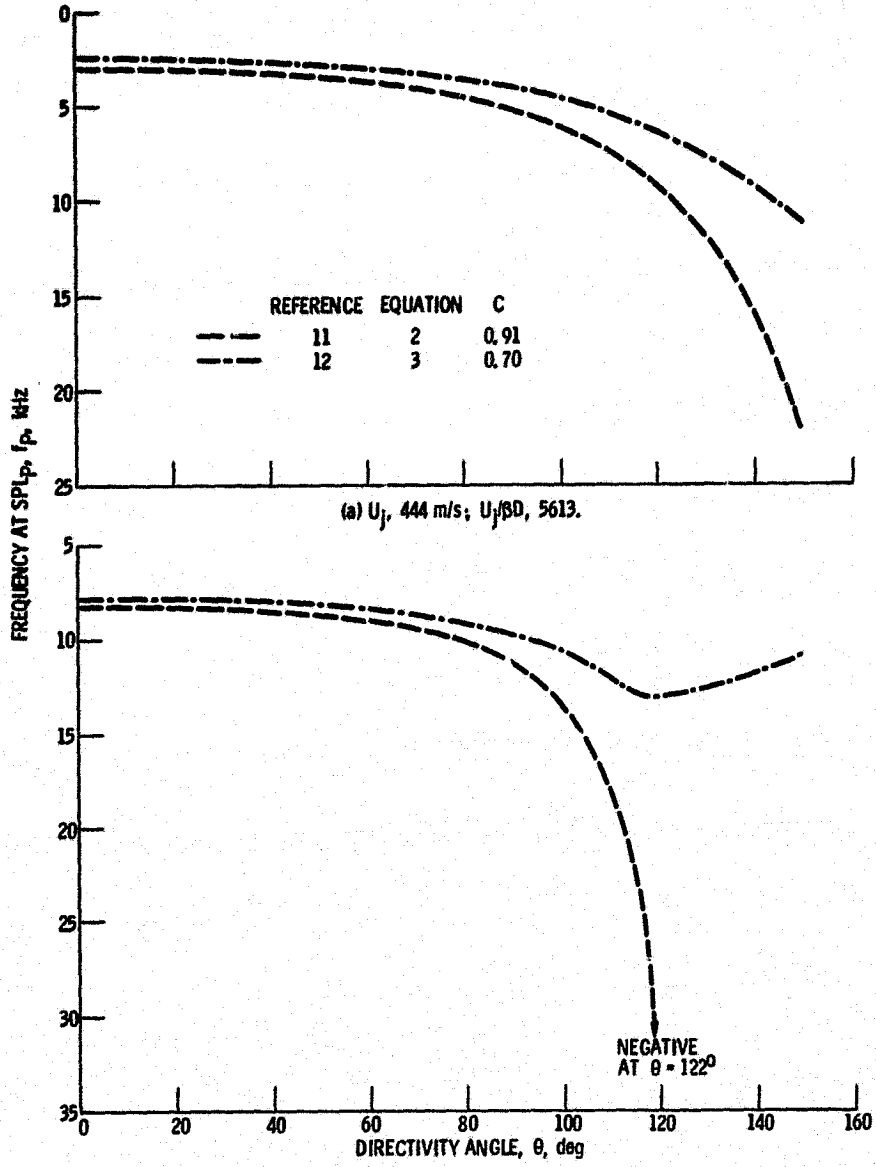

(a) U_j, 444 m/s; $U_j/\beta D$, 5613.

(b) U_j, 922 m/s; $U_j/\beta D$, 11 659.

Figure 4. - Comparison of predictions for frequency at shock-associated SPL$_p$. $\beta = 0.83$; nozzle diam., 9.5 cm.

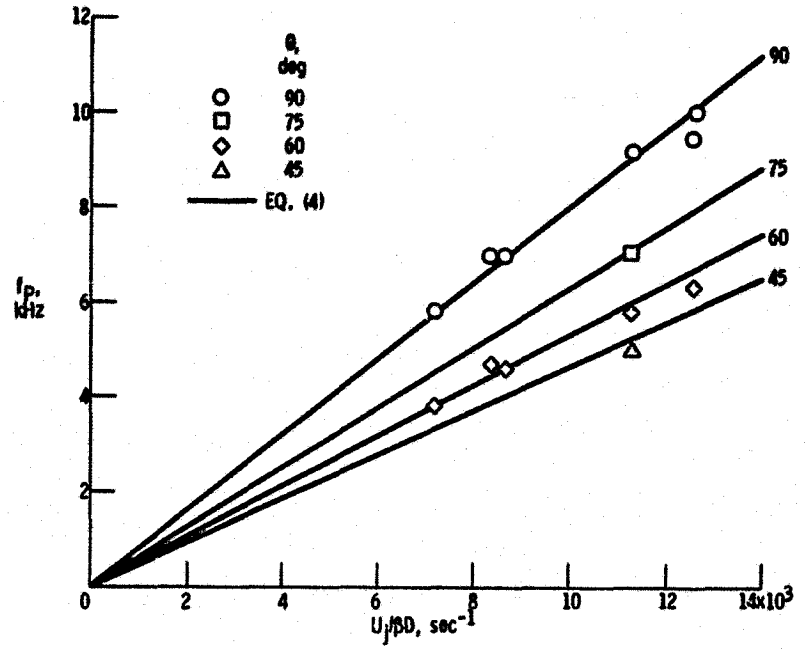

Figure 5. - Correlation of frequency at SPL_p for screech-free shock associated noise. Data from ref. 4.

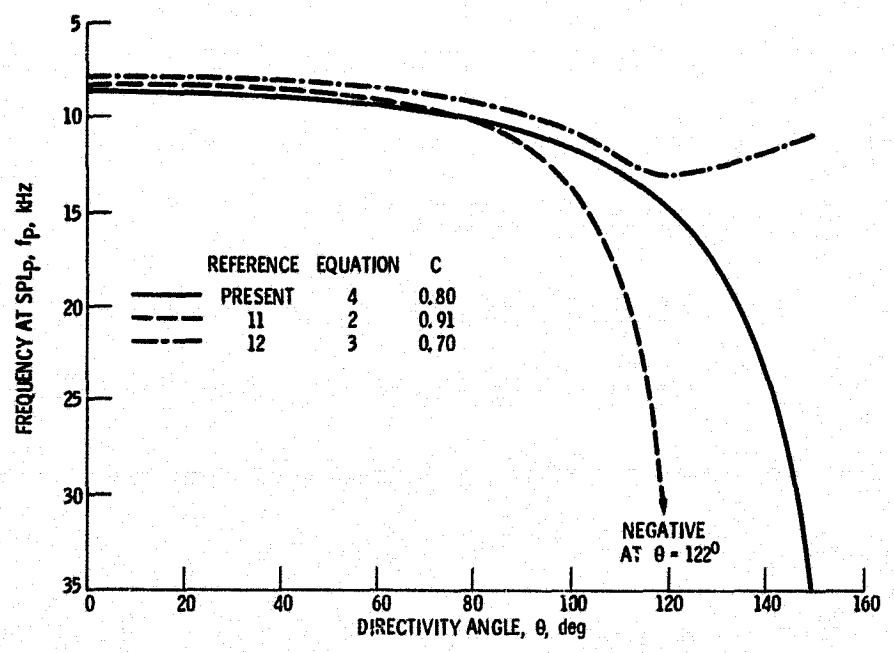

Figure 6. - Comparison of present variation of f_p as a function of θ with those of references 11 and 12. U_j = 922 m/s; $U_j/\beta D$ = 11 659.

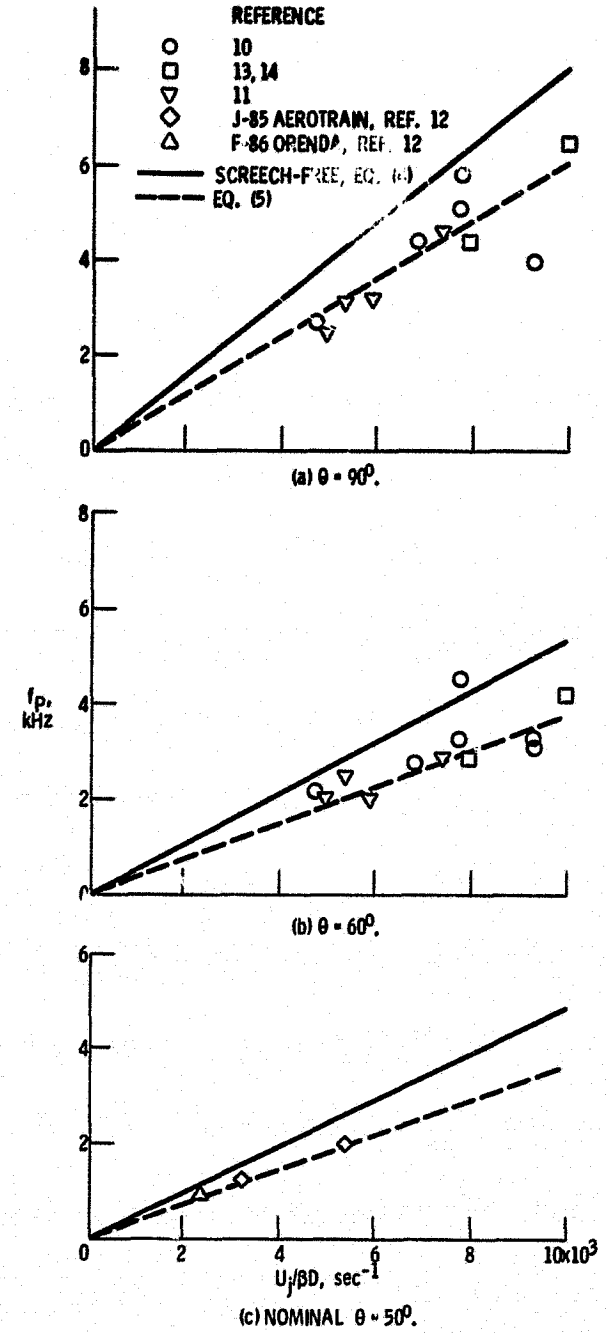

Figure 7. - Comparison of screech-free and screech-contaminated shock noise.

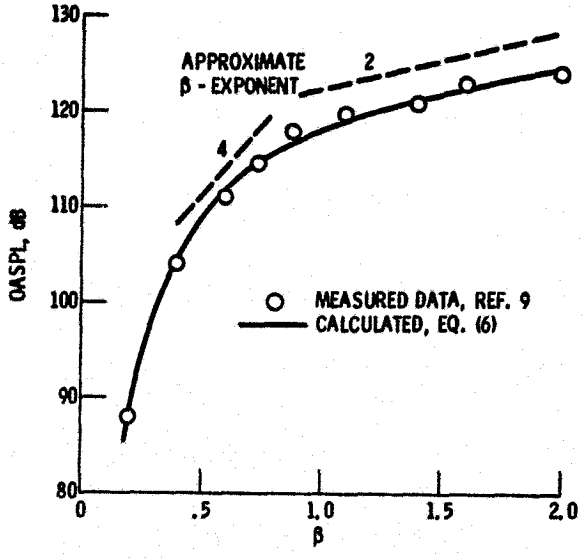

Figure 8. - Overall sound pressure level variation with β. $\theta = 45^{o}$; screech-free data.

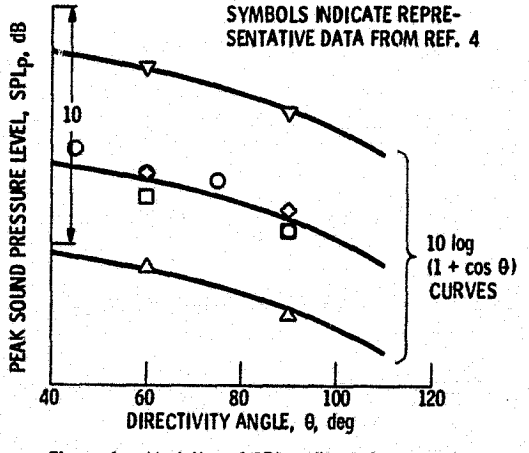

Figure 9. - Variation of SPL_P with θ for screech-free, shock-associated noise for several values of β and T_j/T_o ratios.

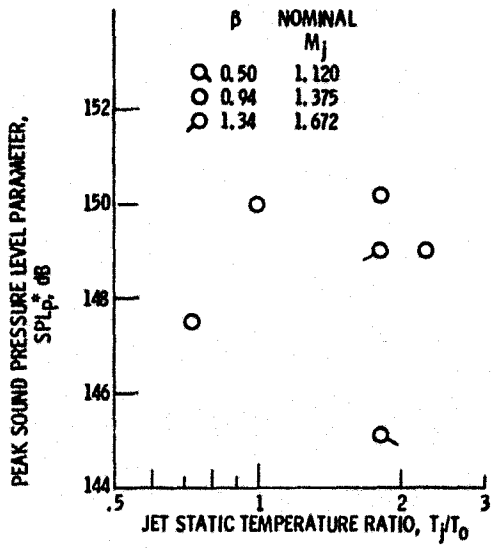

Figure 10. - Variation of SPL_p^* with T_j/T_0 for several values of β. Screech-free data; ref. 4.

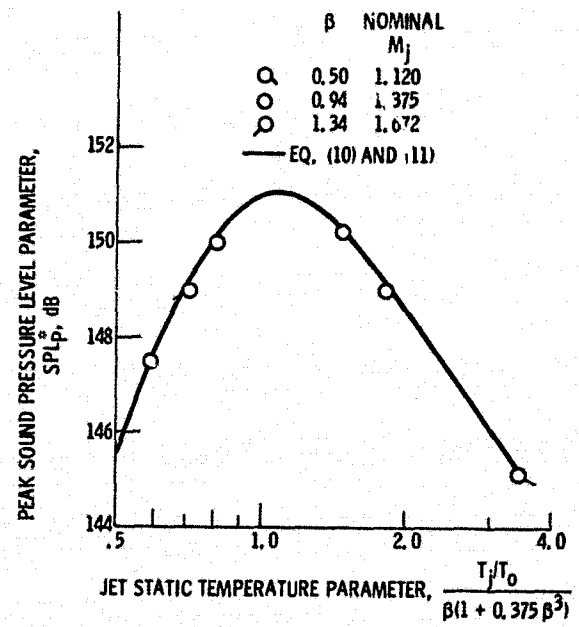

Figure 11. - Correlation of SPL_p^* with T_j/T_0 ratio and β. Screech-free data; ref. 4.

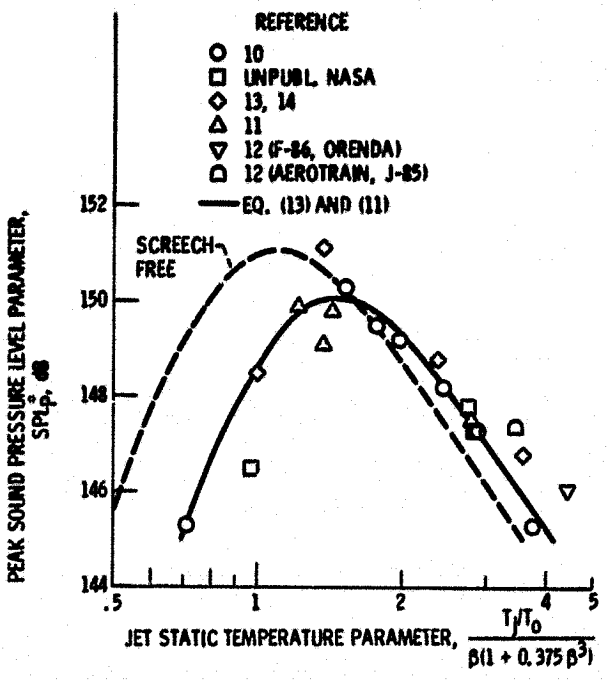

Figure 12. - Correlation of SPL_p^* with T_j/T_0 and β. Screech-contaminated data.

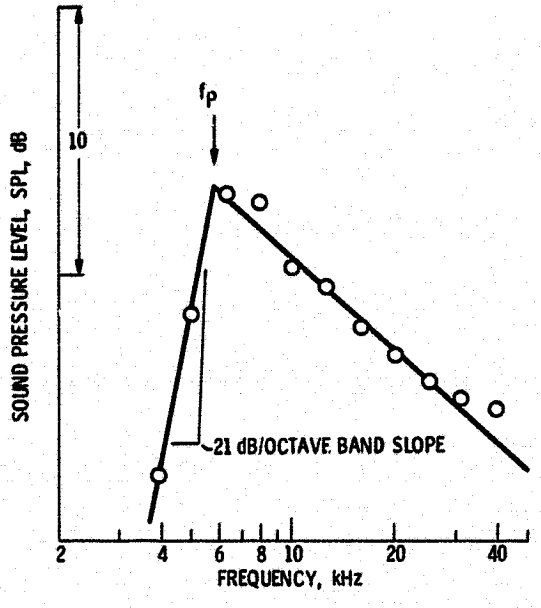

Figure 13. - Representative spectrum of shock-associated noise. $\beta = 0.94$; $T_j/T_0 = 1.82$; $D = 5.1$ cm; $\theta = 60^0$; screech-free; ref. 4.

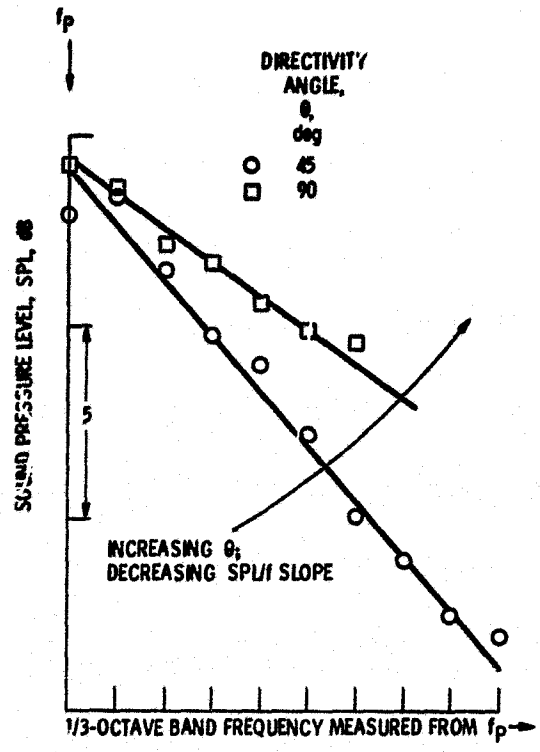

Figure 14. - Typical variation of SPL/f slope in aft portion of spectra with directivity angle. Ref. 4.

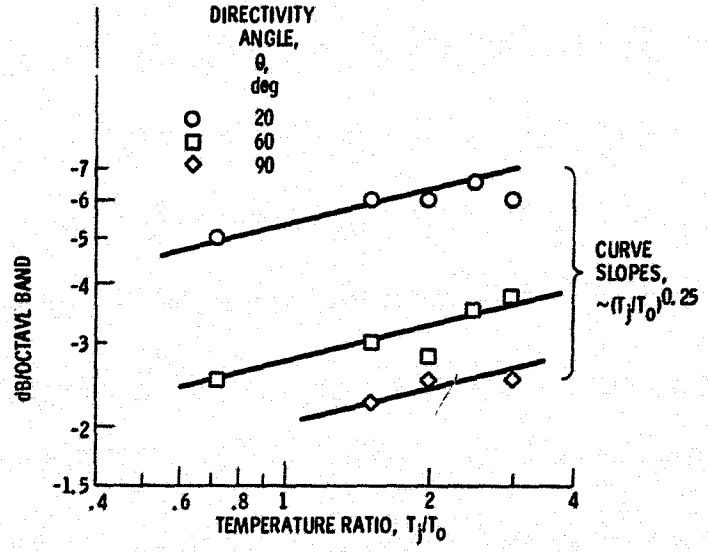

Figure 15. - Typical variation of aft ($f > f_p$) spectral roll-off with temperature ratio, T_j/T_0. Data from ref. 10; $\beta = 0.83$.

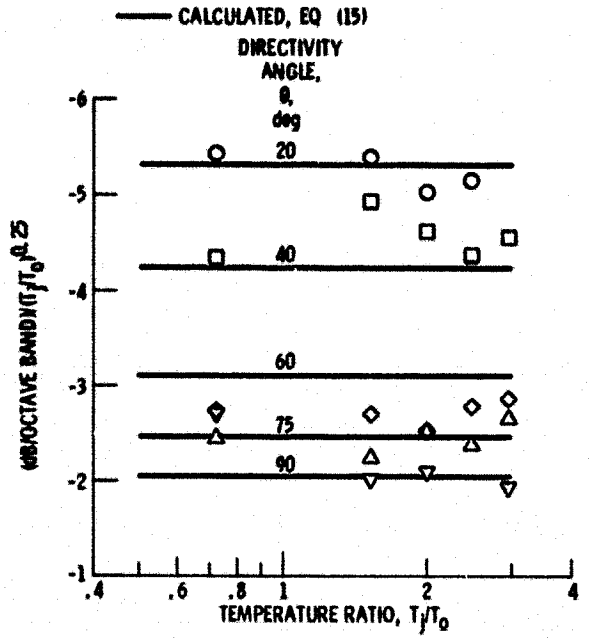

Figure 16. - Comparison of measured and calculated aft spectral roll-off for various directivity angles. Data of ref. 10; $\beta = 0.83$.

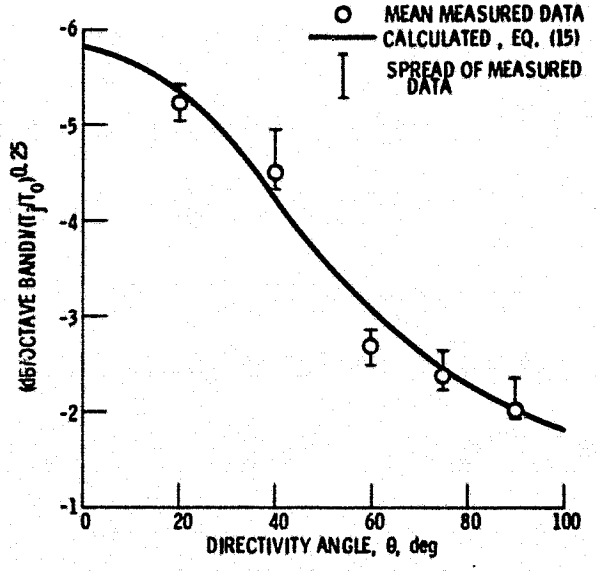

Figure 17. - Variation of aft spectral roll-off parameter as a function of directivity angle. Data of ref. 10; $\beta = 0.83$.

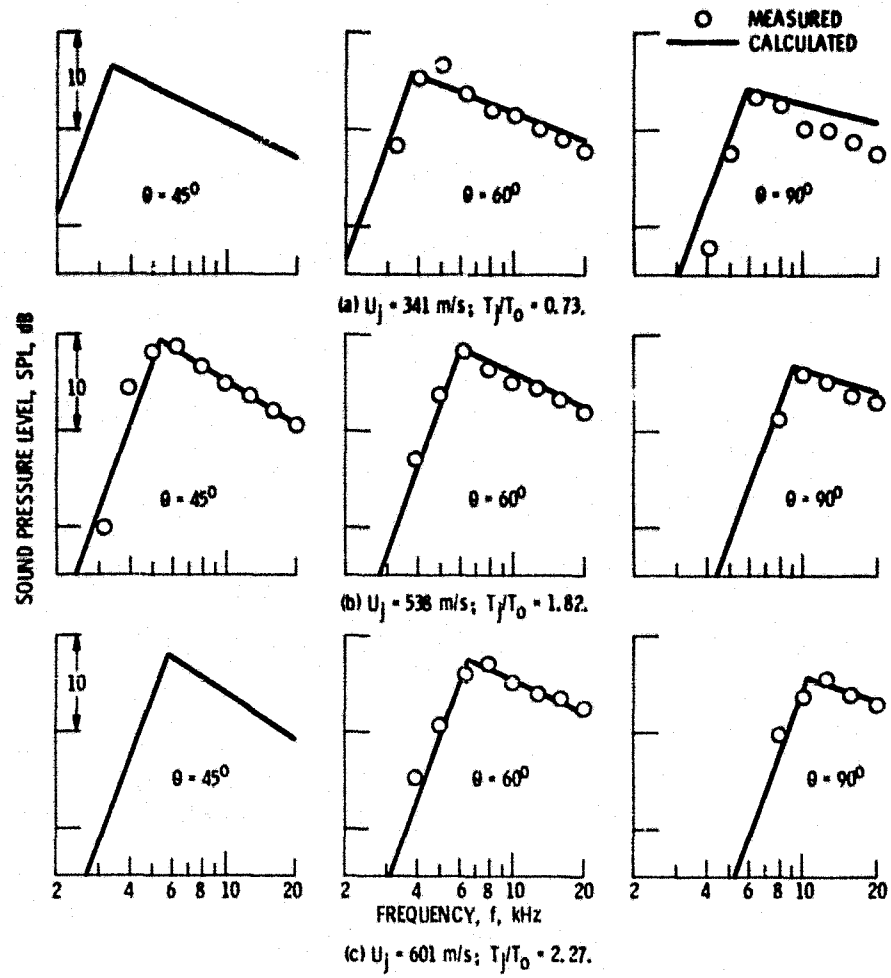

Figure 18. - Comparison of measured and calculated screech-free shock-associated noise at β = 0.94. Data from ref. 4.

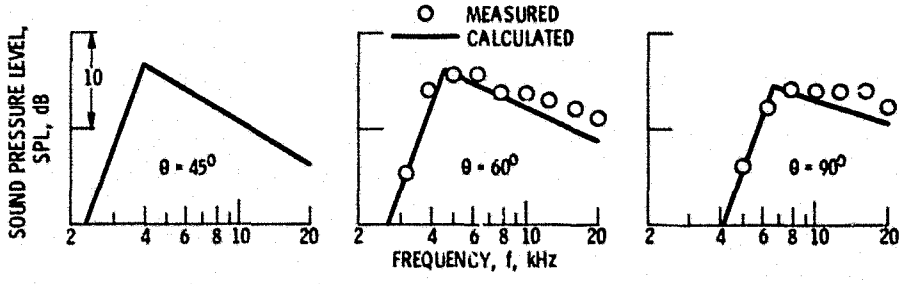

Figure 19. - Comparison of measured and calculated screech-free shock-associated noise at β = 1.34. Data from ref. 4; U_j = 587 m/s; T_j/T_0 = 1.82.

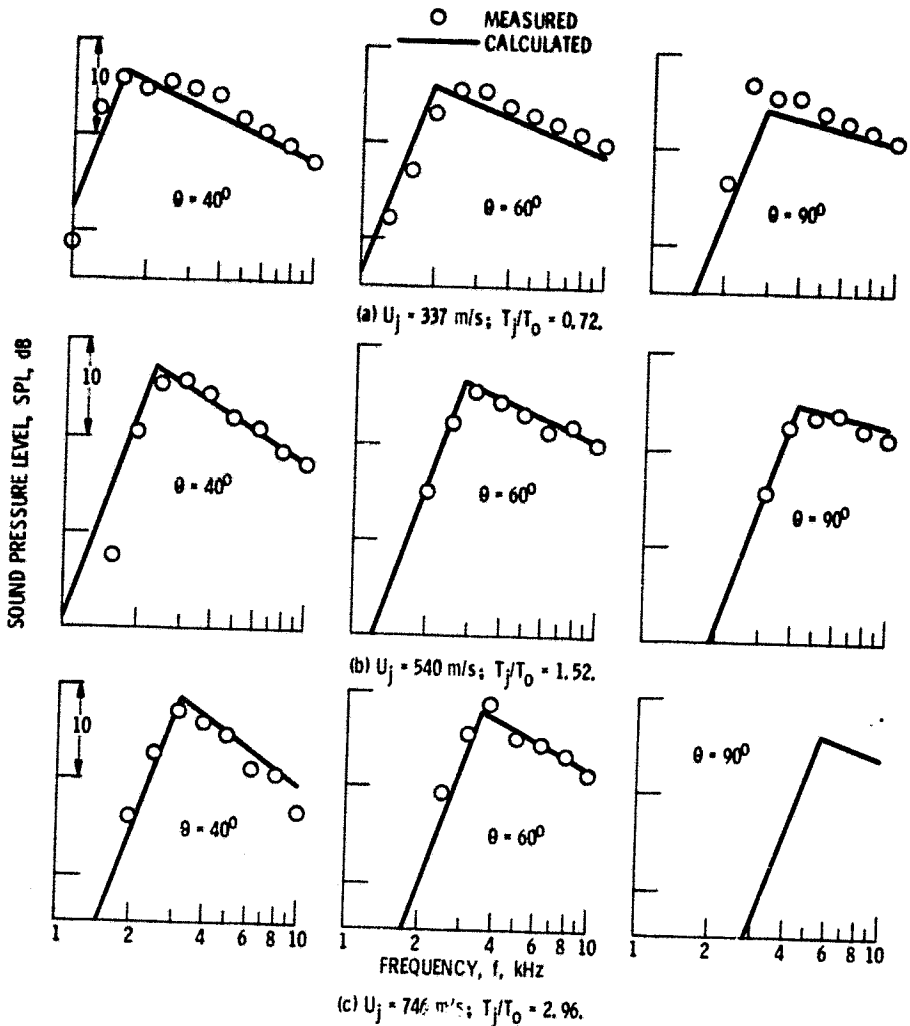

Figure 20. - Comparison of measured and calculated screech-contaminated shock-associated noise at β = 0.83. Data from ref. 10.